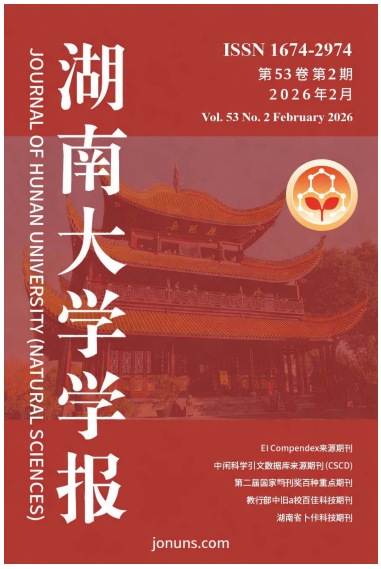

Journal of Hunan University

(Natural Sciences)

Vol. 53 No. 2

February 2026

Available online at

https://jonuns.com

Open Access Article

https://doi.org/10.55463/issn.1674-2974.53.2.3

Hospital Triage Optimization: Evaluation of Machine Learning Models for Blood Pressure Estimation to Enhance Emergency Response in Colombia

Joel Carroll-Vargas [1] *, Andrés Leonardo Jutinico [2], Edwin Alfredo Reyes-Guzmán [3], Andrés Puerto Lara[4]

[1] PhD student in Applied Sciences, Universidad Antonio Nariño, Bogotá, Colombia,
[2] Research professor, Universidad Distrital Francisco José de Caldas, Bogotá, Colombia,
[3] Research professor, Universidad Antonio Nariño, Bogotá, Colombia,
[4] Research, Provectus, San Francisco California, United States,

* Corresponding author: jcarroll37@uan.edu.co

Article History:

Received: January 4, 2026
Revised: February 17, 2026
Accepted: February 24, 2026
Published: March 27, 2026

Abstract Hospital triage requires rapid and accurate assessment of vital signs, supported by well-trained personnel within a robust emergency medical system. However, in remote regions of Colombia, access to skilled staff and monitoring equipment is limited. This study proposes a machine learning framework to estimate blood pressure using photoplethysmography (PPG) signals, demographic data, and comorbidity information within an automated IoT-based triage system. As no prior machine learning–based solutions have addressed patient health status prediction in isolated Colombian regions, this framework aims to provide a complementary triage system in areas lacking expert support. The system integrates a forearm-worn wearable device with a kiosk to collect data, generating 20 input features encompassing demographic/comorbidity information, summary vital signs, and PPG morphology and variability descriptors. Three regression models - feedforward neural network, XGBoost, and Random Forest - are trained and compared for simultaneous estimation of systolic and diastolic blood pressure. Training uses a public short-record PPG dataset comprising 657 signal segments from 219 subjects with subject-wise cross-validation; external validation is performed on the PhysioNet Pulse Transit Time-PPG database. Tree-based ensemble models

outperform the neural network on the main dataset, with XGBoost achieving the best performance for both systolic and diastolic blood pressure. These findings highlight ensemble models as competitive and interpretable alternatives for PPG-based blood pressure estimation, supporting their integration into IoT-enabled triage systems to improve evidence-based patient prioritization, especially in underserved regions.

Keywords Hospital Triage; Machine Learning; Blood Pressure Estimation; Photoplethysmography (PPG); IoT; XGBoost; Random Forest.

医院分诊优化：用于血压估算的机器学习模型评估以提升哥伦比亚急诊响应

摘要：医院分诊需要对生命体征进行快速且准确的评估，这依赖于具备经验的医务人员和完善的急救医疗系统。然而，在哥伦比亚偏远地区，获取熟练人员和监测设备的机会有限。本研究提出了一种基于机器学习的框架，通过光电容积描记法（PPG）信号、人口统计数据和共病信息，在自动化物联网（IoT）分诊系统中估算血压。由于以往尚无针对哥伦比亚偏远地区患者健康状态预测的机器学习解决方案，该框架旨在为缺乏专家支持的区域提供辅助分诊系统。系统将佩戴于前臂的可穿戴设备与信息采集终端结合，生成包括人口统计/共病信息、生命体征汇总以及PPG形态与变异特征在内的20个输入特征。研究训练并比较了三种回归模型—前馈神经网络、XGBoost与随机森林—以同时估算收缩压和舒张压。训练使用包含219名受试者、657段信号的公共短时PPG数据集，并采用受试者交叉验证；外部验证在PhysioNet脉搏传导时间-PPG数据库上进行。结果显示，基于树的集成模型在主数据集上优于神经网络，其中XGBoost在收缩压和舒张压估算上表现最佳。研究结果表明，集成模型在基于PPG的血压估算中具有竞争力且可解释性强，支持其在物联网分诊系统中的应用，以改善基于证据的患者优先分诊，特别是在服务不足的地区。

关键词： 医院分诊；机器学习；血压估算；光电容积描记法（PPG）；物联网（IoT）；XGBoost；随机森林

1. Introduction

Triage is a patient classification process based on severity, using an acuity scale to determine the order of assistance in the emergency department [1]. Therefore, this process is relevant in hospital emergency systems, enabling suitable patient care [2], resource allocation, and ultimately saving lives [3]. The most widely used and referenced triage model worldwide is the Emergency Severity Index (ESI). It is the preeminent system in the United States for classifying the severity of patients' conditions in emergencies. This method allows a comprehensive evaluation that includes pain, specific symptoms, and vital signs [4]. Triage allows for the classification of patients based on selected levels. For instance, in Colombia, the Ministry of Social Protection [5] established five triage levels: Level 1, where the patient requires immediate attention. In this case, the patient's clinical condition is life-threatening and requires resuscitation. Level 2, where the patient's clinical condition may evolve towards rapid deterioration or death or increase the risk of losing a limb or organ, therefore, it requires care that should not exceed thirty minutes. Level 3: The patient is physiologically stable, but their clinical condition requires diagnostic and therapeutic measures in an emergency department. At Level 4, there is a risk of complications or consequences from the illness or injury if the patient does not receive appropriate care. Nevertheless, the patient has medical conditions that do not pose an obvious risk to life or limb or organs. Level 5, the patient presents a clinical condition related to acute chronic problems without evidence of risk to life or the functionality of a limb or organ.

During triage, health professionals develop a rapid assessment of the patient's airway, ventilation, and circulation. They made a series of specific questions to

determine the reason for the urgency. Also, the patient's vital signs are evaluated, including temperature, heart rate, respiratory rate, and blood pressure. In addition, the treatment area is designated within the emergency service according to the patient's priority. However, in isolated regions of Colombia and other developing countries, there is a lack of healthcare services, and sometimes there is no health center with experts who can perform emergency triage assessments. On the other hand, considering that access to information and communication technologies has increased in these countries over the last decade, it is pertinent to develop a system that supports experts by using information and communication technologies and computational intelligence to predict patients' health status. Therefore, this article presents the estimation of blood pressure using machine learning algorithms for a triage system that can be deployed in isolated regions.

Triage promotes the efficient use of healthcare resources in a high-pressure, time constrained environment. By swiftly identifying patients requiring immediate attention, medical staff can focus on stabilizing critical cases and preventing further deterioration. The above increases the chances of survival for the most severely affected and improves the overall functioning of the healthcare system by preventing it from becoming overwhelmed [6]. Therefore, triage also prevents delays in treating patients with less severe conditions. By classifying patients into different levels of urgency, the aim is to ensure that all patients receive timely care according to their need [7] s. Additionally, triage contributes to more efficient, organized patient flow within the hospital [8]. However, research from the past decade has shown that sometimes current triage methods are ineffective in accurately identifying patients who require life-saving interventions. For example, in [9] reports discrepancies in the classification establishment between the medical emergency dispatch center and ambulance teams and reports of poor classifications causing dissatisfaction among the patients' relatives [10].

In the literature, there are several proposals for continuous blood pressure estimation using photoplethysmography (PPG) signals and their correspondence with electrocardiogram (ECG) signals, either by measuring the pulse wave velocity (PWV) or the pulse transit or arrival time (PTT/PAT) [11], [12], [13]. The research developed in [14] presents a method for measuring systolic and diastolic blood pressure using recordings of Korotkoff sounds and a convolutional neural network (CNN). The neural network training data were obtained from nine measurements taken with variations in stethoscope position and pressure on 30 healthy subjects. The estimation of diastolic and systolic blood pressure achieved mean errors (MEs) of 3.3 and 1.4, respectively. The study showed that models based on Korotkoff sounds and convolutional neural networks (CNNs) can be affected by delays and variations in sound capture (e.g., differences in stethoscope position or observer response time), introducing systematic errors in blood pressure estimation. The authors of [15] compared k-nearest neighbors (KNN), weighted KNN, and decision trees algorithms for estimating blood pressure. The dataset included 155 subjects and diastolic and systolic blood pressure measurements obtained by manual assessment of Korotkoff sounds. The results indicated mean absolute errors (MAEs) of 3.6, 3.5, and 4.5 for systolic blood pressure, respectively. In contrast, the diastolic blood pressure estimation yielded MAEs of 11.1, 11.0, and 13.1, respectively, which are higher than those reported in [14]

2. Methods

2.1. Triage Protocols and Vital Sign Definitions

The Pan American Health Organization (PAHO) has published a manual for the implementation of a triage system in emergency rooms, based on the Canadian Triage and Acuity Scale (CTAS) model. This manual provides a practical guide for emergency medical services managers and professionals, with the aim of improving the quality and efficiency of care [16]. Likewise, in Colombia, the Ministry of Health and Social Protection establishes the rules and criteria for the application of triage in the country's emergency services through Resolution 5596 of 2015[5]. In this paper, we introduce an approach to an automatic triage system that can be deployed in isolated regions, considering the above rules and criteria. The automatic triage device consists of a computerized kiosk that registers demographic and comorbidity data and measures vital-sign. The vital signs are the body temperature and signals measured by a PPG sensor: heart rate, peripheral capillary oxygen saturation (SpO2), respiratory rate surrogate, heart-rate variability index, and perfusion index. The demographic and comorbidity data are: age, weight, or a binary indicator of previously diagnosed arterial hypertension, diabetes mellitus, and other relevant chronic diseases reported by the patient. Also, the device estimates blood pressure using computational intelligence algorithms, vital-sign measurements, and demographic and comorbidity data. To aid the reader's understanding, we highlight the following definitions within the proposed approach:

SpO2 – The level of oxygen in the blood is measured by a photoplethysmography sensor, which detects changes in the absorption of near-infrared light by

vascularized tissues, typically on the wrist or forearm. Oxygenated and deoxygenated hemoglobin in the blood absorb different wavelengths of light, causing variations in the amount of light reaching the photodiode sensor in response to heartbeats. These fluctuations are electronically processed to calculate the blood oxygen saturation level (SpO2), thereby providing a non-invasive and rapid measurement of blood oxygenation as a percentage.

Body temperature – An infrared temperature sensor measures the temperature of the human body without direct contact by detecting the infrared radiation emitted by the skin. When the sensor is aimed at the forehead or the ear, it captures the infrared radiation, converts it into an electrical signal, and estimates the body temperature using calibration algorithms that take into account the skin's emissivity. If the measured temperature exceeds a pre-set threshold, typically 100.4◦F or 38◦C, the sensor indicates fever. Since the wrist, where the wearable device is installed, is not a suitable location for measuring body temperature, it is necessary to design a kiosk (see Figure 3) to measure body temperature, among other functions.

Figure 1. The automatic triage use a kiosk that measures vital-sign and registers demographic and comorbidity data

Heart rate – As the heart beats, the amount of blood in the blood ves- sels changes within the measured area, affecting the absorption of light by hemoglobin. The variations in light absorption translate into fluctuations in the signal captured by the sensor, known as a pulse wave. By electronically processing these fluctuations, the photoplethysmography sensor can accurately determine the individual's heart rate, thus providing a non-invasive and real time measurement of cardiac activity.

Blood pressure – The measurement of diastolic and systolic blood pressure in humans by PPG is currently a scientific challenge, mainly due to the low accuracy of devices other than cuff-based systems [17], [18], [19],[20] The Pan American Health Organization defines blood pressure as the force exerted by blood against the walls of blood vessels (arteries) as a result of the heart's pumping function, blood volume, arterial resistance to flow, and artery diameter [21]. Blood pressure is expressed with two values: the systolic pressure, which corresponds to the moment when the heart contracts or beats, and the diastolic pressure, which represents the pressure exerted on the vessels when the heart relaxes between beats[22]. These values are measured in millimeters of mercury (mmHg).

2.2 Design of the wearable device for emergency department hospital triage

The system comprises three main components within the application domain. As shown in Figure 2, these components include a device attached to the patient's arm, which integrates communication modules and an expert decision-support system. All devices are wirelessly connected to the emergency data center through Wi-Fi, enabling efficient data transmission to the gateway connected to the cloud server. This centralized structure allows fast and secure access to medical information from any location. The combination of IoT devices and communication technologies streamlines clinical decision-making for both medical professionals and patients, providing real-time data and storing it for long-term analysis. Together, these elements enhance the quality of care, especially in critical situations. Figure 2 depicts the architecture of a triage system based on IoT devices and cloud computing, organized into three functional layers. In Layer 1 **Data collected**, the patient's physiological data are acquired by a wearable device that communicates via Wi-Fi with a terminal or kiosk. In Layer 2 **Gateway**, this terminal acts as a gateway, aggregating the information and securely uploading it to the cloud. The central part illustrates the **IoT cloud computing** block, where the data are processed by clinical decision-support algorithms. Finally, in Layer 3 **Healthcare providers**, the analysis results are mapped to different priority levels (risk, urgent, sick, cold case, and normal), which are communicated to healthcare staff and hospital infrastructure to optimize the triage process in the emergency department.

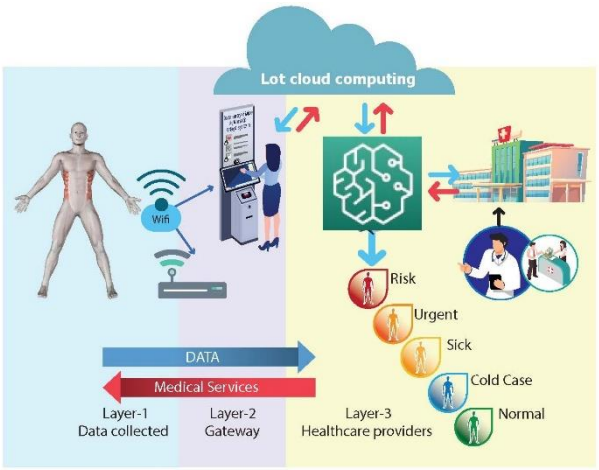

Figure 2. General architecture. Diagram showing the three-layer system architecture for the automated triage system. Layer 1 includes data acquisition from wearable. sensors, Layer 2 processes and classifies the data, and Layer 3 displays triage outcomes for healthcare providers via a cloud-based platform.

The system integrates an advanced neural network that estimates blood pressure by combining demographic data such as age, weight, and gender with the photoplethysmography signal, enabling accurate and personalized measurements. Using the same sensor, the system also captures and analyzes the patient's heart rate, blood oxygen levels, and body temperature, providing a comprehensive real-time assessment of their physiological state and facilitating more informed and effective medical care. The triage bracelet is a device worn on the patient's forearm, containing sensors to measure heart rate, blood oxygen saturation, arm movement, and arm acceleration. These data are transmitted to an external device via Wi-Fi, where they are used to assess the patient's condition and prioritize medical attention. Figure 3 illustrates the device placed on the patient's arm.

Figure 3. Wearable device overview. Image of the forearm-worn wearable device pro totype used for capturing physiological data, including heart rate, SpO2, temperature, and motion. It shows sensor placement and communication modules embedded in the device.

For the prototype, a compact microcontroller module was selected, offering the main functionalities of the ESP32 DEVKIT V1 in a reduced form factor and integrating a TP4057 controller for charging 3.7 V lithium batteries. The MAX86150EFF+T digital PPG sensor was connected via the I2C communication protocol through the designated ports. In addition, an analog PPG sensor was connected to one of the module's analog inputs. Power was supplied by a 3.7 V lithium battery through the integrated charging interface. The schematic representation of the configuration and hardware is shown in Figure 4. Subsequently, a casing was designed and built to protect the electronics and support the bracelet. The following image shows the system attached to a person's arm, as is shown in Figure 5

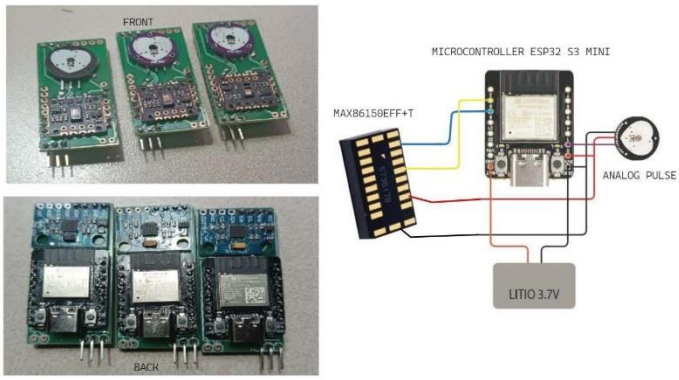

Figure 4. The schematic diagram clearly illustrates the connections: the MAX86150EFF+T sensor is interconnected through the microcontroller's I2C lines (SDA and SCL). The analog pulse sensor connects directly to an analog input port. A 3.7 V lithium battery is connected to the dedicated battery charging terminals on the microcontroller.

Figure 5. The image depicts a practical implementation of the device on a user's arm. The bracelet-like enclosure securely houses the electronic components and sensors, facilitating comfortable and continuous biometric data acquisition.

2.3 Feature extraction for blood pressure estimation from PPG signals

The system integrates an advanced neural network that estimates blood pressure from a set of 20 input features. These features are grouped into three categories: (i) demographic and comorbidity data

collected at the kiosk (age, sex, weight, history of hypertension, history of diabetes, cerebral infarction and cerebrovascular disease); (ii) summary vital sign measurements extracted from the wearable device (such as heart rate, and body mass index (BMI)); and (iii) Engineered features of PPG segments, waveform mean, standard deviation and Root Mean square PPG values.

The relationships among all variables are shown in the Pearson correlation matrix (Figure 6), which highlights degrees of association, potential redundancies, and informs feature selection. Importantly, the features listed in Table 1, together with the relevant demographic and clinical variables depicted in Figure 6, constituted the common input set used to train and evaluate all three models (feedforward neural network, Random Forest, and XGBoost), ensuring a consistent basis for comparative analysis.

The correlation matrix shows that the strongest associations are observed between body weight and BMI, as well as between systolic and diastolic blood pressure, which is consistent with cardiovascular physiology. High positive correlations are also evident among segments 1, 2, and 3, suggesting that they represent closely related features derived from the same underlying signal. Clinically, age exhibits a notable correlation with the presence of hypertension and cerebrovascular disease (cerebral infarction), while diabetes is also positively associated with cerebrovascular disease. In contrast, subject height shows only very weak correlations with the remaining variables and was therefore excluded from subsequent analyses. Overall, the remaining variables display correlations of lower magnitude, both positive and negative, indicating weaker or more indirect relationships within the analyzed dataset.

2.4 Subject-wise cross-validation and independent generalization assessment

This study presents the training and evaluation of a deep neural network, an XG- Boost, and a random forest algorithms for blood pressure estimation within an auto-
mated triage system. The model integrates key emographic and physiological variables, such as age, sex, and weight, along with features derived from pulse waveforms (PPG). Training was performed on the publicly available Health Dataset for the NonInvasive Detection of Cardiovascular Diseases, The PPG-BP dataset, collected at Guilin People's Hospital, comprises 219 adult participants and 657 PPG segments, three per subject. Each segment is a short 2.1 s recording 2100 samples acquired at 1 kHz with 12-bit resolution using a portable acquisition setup, PPG probe, microcontroller, and smartphone app, while arterial blood pressure was measured with an Omron HEM-7201 device; PPG and blood pressure were obtained in close succession within an approximately 3 min window total experimental session 15 min segment_1, segment_2, and segment_3. The dataset is distributed as 219 subject folders, three PPG files per subject together with a spreadsheet PPG-BP database.xlsx containing variables such as sex, age, height, weight, systolic/diastolic blood pressure, heart rate, and comorbidities [23]. Model performance and generalization were obtained via stratified k-fold cross-validation and external evaluation against the PhysioNet Pulse Transit Time–PPG database [24], see Figure 7.

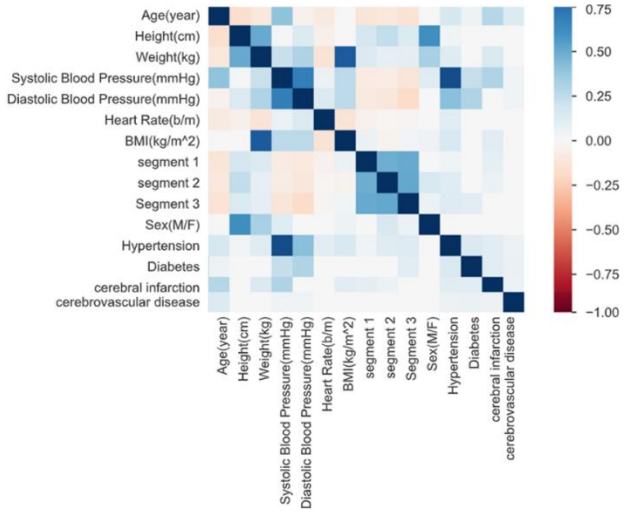

Figure 6. Correlation matrix Pearson's r among the study's input variables. Warm colors denote positive correlations and cool colors negative ones; color intensity encodes the magnitude $|r|$.

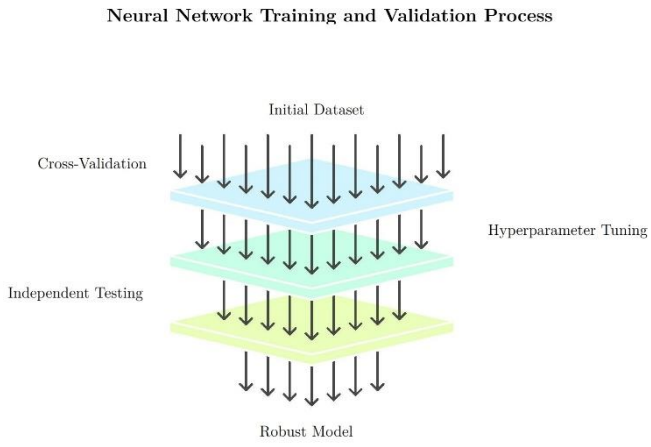

Figure 7. The image illustrates a machine learning model development workflow where an initial dataset undergoes cross-validation, hyperparameter tuning, and evaluation with an independent set, culminating in a robust and generalizable model ready for deployment.

Table 1. Types of features used as inputs to the neural network for blood pressure estimation.

Group	Feature	Description
(i) Demographic and comorbidity data (kiosk)		
1	Age (years)	Patient age in years.
2	Sex	Biological sex (e.g., male/female), encoded as a categorical variable.
3	Weight (kg)	Patient body weight measured at the kiosk.
4	History of hypertension	Binary indicator of previously diagnosed arterial hypertension.
5	History of diabetes	Binary indicator of previously diagnosed diabetes mellitus.
6	Cerebral infarction	Binary indicator of other relevant chronic diseases reported by the patient.
7	Cerebrovascular disease	Binary indicator of other relevant chronic diseases reported by the patient
(ii) Summary vital-sign measurements and wearable device indices		
7	Heart rate	PPG signal peaks per minute counter
8	BMI	weight (kg) / height (m²)
(iii) Engineered features		
12	Mean PPG value Segment_1	Average PPG amplitude over the analysis window corresponding to Segment 1.
13	Mean PPG value Segment_2	Average PPG amplitude over the analysis window corresponding to Segment 2
14	Mean PPG value Segment_3	Average PPG amplitude over the analysis window corresponding to Segment 3
15	SD PPG value Segment_1	Standard Deviation PPG amplitude over the analysis window corresponding to Segment 1
16	SD PPG value Segment_2	Standard Deviation PPG amplitude over the analysis window corresponding to Segment 2
17	SD PPG value Segment_3	Standard Deviation PPG amplitude over the analysis window corresponding to Segment 3
18	RMS PPG value Segment_1	Root Mean Square PPG amplitude over the analysis window corresponding to Segment 1
19	RMS PPG value Segment_2	Root Mean Square PPG amplitude over the analysis window corresponding to Segment 2
20	RMS PPG value Segment_3	Root Mean Square PPG amplitude over the analysis window corresponding to Segment 3

2.5 Deep Neural Network for Blood Pressure Estimation

A feedforward neural network was implemented for the simultaneous prediction of systolic and diastolic blood pressure from the 20 input features described in Table 1. These features combine demographic and comorbidity information collected at the kiosk with summary vital-sign measurements and morphology/variability descriptors derived from the PPG waveform. All covariates were standardized using a z-score fitted on the training set and applied to the validation and test splits. The architecture, implemented in PyTorch, comprises fully connected layers with sizes $n_{inputs}= 20 - 256 - 64 - 32 - 16 - 2$. ReLU activations are applied after each hidden layer, while the final output layer remains linear (no activation), so the model has nonlinear representational capacity and is not equivalent to a multivariate linear regression. The problem is formulated as a multi-output regression (two linear output neurons) and is trained with the L1 loss (MAE) and the Adam optimizer (learning rate $1x10^3$) for 200 epochs. During training, both training and validation errors are monitored (the test set is held out and evaluated once at the end). After training, MAE, RMSE, and R^2 are computed on the test set, together with observed–predicted comparisons. Figure 8 depicts the implemented network, which takes as input the 18 features grouped into demographic/comorbidity data, summary vital-sign measurements, and PPG morphology/variability descriptors.

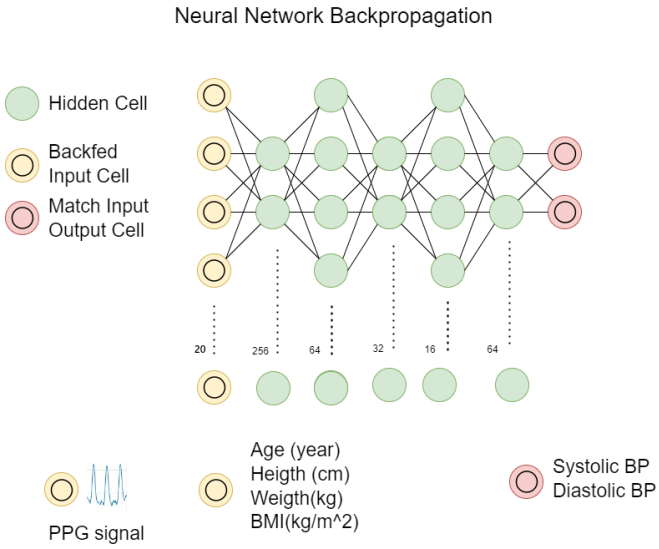

Figure 8. Neural Network Architecture. Graphical representation of the feedforward neural network used for blood pressure estimation.

In Figure 8, $w_{ji}^{(l)}$ represents the weight that controls the strength of the connection between neuron i in layer $l-1$ and neuron j in layer l, while $y_i^{(l-1)}$ denotes the input received from neuron i in the previous layer (with $y^{(0)} = x$ the network input). The term $\theta_j^{(l)}$ corresponds to the bias of neuron j in layer l, which allows shifting its activation. For each layer l, n_{l-1} denotes the number of inputs received from the previous

layer. The quantity $u_j^{(l)}$ is the net input to neuron j in layer l, computed as a weighted sum of the outputs of the previous layer minus the bias, as defined in Equation (1). The output $y_j^{(l)}$ is then obtained by applying the activation function $g^{(l)}(\cdot)$ to $u_j^{(l)}$, as shown in Equation (2). The activation function introduces nonlinearity into the model, enabling the network to learn and represent complex relationships between the input features and the final output.

$$u_j^{(l)} = \sum_{i=1}^{n_{l-1}} w_{ji}^{(l)}\, y_i^{(l-1)} - \theta_j^{(l)}, \quad j = 1, \ldots, n_l \tag{1}$$

$$y_j^{(l)} = g^{(l)}\left(u_j^{(l)}\right), l = 1, \ldots, L, \quad j = 1, \ldots, n_l \tag{2}$$

2.6 XGBoost Model

In boosting, a strong predictor is built additively from weak learners trained in successive rounds that emphasize harder examples (i.e., those with larger errors in previous iterations); each new learner corrects residuals or, more generally, follows the gradient of the loss and the final prediction is the (weighted) sum of all learners, which improves performance for classification and regression tasks[25]. XGBoost is a gradient-boosting realization with classification and regression trees (CART) that formalizes this as an additive model The mathematical expression is shown in Equation 3.

$$Z = F(x_i) = \sum_{t=1}^{T} f_t(x_i), \tag{3}$$

In this formulation, $x_i \in R^p$ denotes the feature vector of example i, with p input variables. $F(\cdot)$ is the ensemble predictor and Z denotes the model output (prediction) for x_i , $f_t(\cdot)$ is the prediction function of the $t-$ th CART tree, weak learner and T is the total number of trees added sequentially.

$$\hat{y}^{(t)} = \hat{y}^{(t-1)} + \eta\, f_t(x) \tag{4}$$

At boosting iteration t, the model prediction for sample i is updated as:

$$\hat{y}_l^{(t)} = \hat{y}_l^{(t-1)} + \eta\, f_t(x_i), \tag{5}$$

where $\hat{y}_l^{(t)}$ and $\hat{y}_l^{(t-1)}$ denote the current and previous predictions, respectively, $f_t(x_i)$ is the prediction of the newly added regression tree f_t, and $\eta \in (0,1]$ is the learning rate (shrinkage parameter) that controls the contribution of the new tree. Smaller values of η typically require a larger number of trees T but tend to improve generalization. Unlike AdaBoost, which updates example weights based on the classification error, XGBoost directly minimizes a regularized objective using a second–order Taylor expansion of the loss $l(y_i, \hat{y}_i)$ around the current prediction. For each training example i, it computes the first- and second-order derivatives

$$g_i = \frac{\partial l(y_i, \hat{y}_i)}{\partial \hat{y}_i}, \; h_i = \frac{\partial^2 l(y_i, \hat{y}_i)}{\partial \hat{y}_l^{\,2}}, \tag{6}$$

which correspond to the gradient and Hessian of the loss. For a candidate split, these quantities are aggregated over the parent node P and its left and right children L and R as

$$G_* = \sum_{i \in *} g_i\,, H_* = \sum_{i \in *} h_i\,, * \in \{P, L, R\}. \tag{7}$$

The quality of a split is then evaluated by the regularized gain

$$\text{Gain} = \frac{1}{2}\left(\frac{G_L^2}{H_L+\lambda} + \frac{G_R^2}{H_R+\lambda} \frac{G_P^2}{H_P+\lambda}\right) - \gamma, \tag{8}$$

where $\lambda \geq 0$ is the l_2 regularization parameter on leaf weights, which stabilizes the estimates when H_* is small, and $\gamma \geq 0$ is the minimum loss reduction required to perform a split, acting as a complexity penalty on the number of leaves. Given a fixed tree structure, the optimal weight assigned to leaf j has the closed form

$$w_j^\star = -\frac{G_j}{H_j + \lambda}, \quad (9)$$

where G_j and H_j denote the sums of gradients and Hessians over the samples that fall into leaf J. The corresponding regularization term for a tree f is

$$\Omega(f) = \gamma T + \frac{1}{2}\lambda \sum_{j=1}^{T} w_j^2, \quad (10)$$

which penalizes both the number of leaves (through γ) and large leaf weights (through λ). Optional l_1 regularization with parameter α can be incorporated by applying soft-thresholding to G_j before division by $H_j + \lambda$, thereby encouraging sparsity in the leaf weights.

Model capacity and the bias variance trade-off are governed by the number of trees and learning rate ($n\_estimators, learning\_rate = \eta$); structural complexity is controlled by depth and node/ leafconstraints (max_depth, min_child_weight, a lower bound on H_j, and gamma $= \gamma$); and stochastic subsampling over rows/columns (subsample, colsample_bytree/colsample_bynode/colsample_ bylevel) improves generalization and efficiency. Modern implementations (tree_method=hist with quantile sketches) accelerate training, handle missing values. Altogether, XGBoost's architecture an additive ensemble of shallow trees optimized by second-order methods with explicit structural penalty yields an efficient, controllable estimator well suited to continuous targets such as systolic and diastolic blood pressure.

2.7 Random Forest

We implemented a multi-output *Random Forest Regressor* to predict systolic and diastolic blood pressure (SBP, DBP) from photoplethysmography (PPG) descriptors fused with clinical covariates. Mathematically, the forest estimates the vector response shown in Eq.(11) and aggregates T decision trees trained on bootstrap samples as in Eq. (12); each tree (f_t) partitions the feature space by maximizing the reduction in squared error (variance) aggregated across outputs, and each leaf returns the vector mean of the targets within its region.

$$\hat{y} = \left[\widehat{SBP}, \widehat{DBP}\right] \quad (11)$$

$$\hat{y}(x) = \frac{1}{T}\sum_{t=1}^{T} \mathrm{b} f_t(x)$$

In the PyTorch-based implementation, the model ingests the same 18 covariates described in Section 2.3, 2.4 and Table 1, combining demographic and comorbidity variables collected at the kiosk (age, sex, weight, history of hypertension, diabetes, and other chronic conditions), summary vital-sign indices from the wearable (heart rate, SpO_2, body temperature, respiratory-rate surrogate, heart-rate variability index, perfusion index), and morphology/variability descriptors of the PPG waveform (mean value, standard deviation, pulse-wave amplitude, systolic upstroke time, diastolic time, and a signal-quality index). Continuous predictors were standardized using a z-score fitted on the training folds, whereas categorical variables were encoded via one-hot representations, ensuring that all models were trained on an identical feature space. A random forest regressor with 100 trees, trained within the PyTorch pipeline (bootstrap sampling, squared-error criterion, unconstrained depth), exploited the native multi-output formulation to jointly predict SBP and DBP as in (8)-(9). Model performance was summarized using MAE, RMSE, and (R^2), computed under the subject-wise cross-validation and independent external evaluation protocol detailed in Section 2.4.

3. Result

The results are presented in Tables 2 and 3, which show the performance of the models for these metrics.

Table 2. Result systolic blood pressure

Model	RMSE	MAE	R²
Back Propagation	8.952	7.194	0.862
XGBoosting*	6.097	5.505	0.928
Random Forest	6.829	5.514	0.915

*Obtained improved outcomes

Table 3. Result diastolic blood pressure

Model	RMSE	MAE	R²
Back Propagation	7.840	5.666	0.712

Model	RMSE	MAE	R^2
XGBoosting*	7.356	5.704	0.758
Random Forest	7.621	5.921	0.781

The evaluation results for systolic and diastolic blood pressure estimation show that tree-based ensembles generally offer the strongest overall performance especially for systolic BP although the best metric varies by model for diastolic BP. For systolic BP, XGBoosting delivers the best results across all metrics (RMSE = 6.097 mmHg, MAE = 5.505 mmHg,($R^2 = 0.928$), followed by Random Forest (RMSE = 6.829 mmHg, MAE = 5.514 mmHg,($R^2 = 0.915$), while Back Propagation trails behind (RMSE = 8.952 mmHg, MAE = 7.194 mmHg,($R^2 = 0.862$). For diastolic BP, the picture is mixed: XGBoosting attains the lowest RMSE (7.356 mmHg), Random Forest achieves the highest (R^2) (0.781), and Back Propagation yields the lowest MAE (5.666 mmHg). Notably, all models keep diastolic RMSE below 8 mmHg, and the two ensemble methods are also below this threshold for systolic BP, supporting the practical viability of ensemble approaches for non-invasive BP estimation from PPG signals.

4. Discussion

This discussion presents an analysis of the results of this study, comparing them with non-invasive blood pressure estimation reported in scientific literature. Here, we consider the RMSE, MAE, and R^2 indices, which provide a more comprehensive evaluation of error dispersion and generalizability. Notice that these indices are critical for clinical validation and the adoption of these solutions in triage systems of isolated regions. The comparative analysis in Table 4 situates the proposed XGBoosting model within the context of state-of-the-art blood pressure estimation approaches. Classical algorithms such as KNN, Weighted KNN, and Bagged Trees [15] report low MAE values for systolic BP estimation 3.590, 3.520, and 4.499 mmHg, respectively. However, the absence of RMSE and R^2 indices in these studies limits a complete assessment of generalization and error dispersion. Similarly, CNN-based methods leveraging Korotkoff sounds [14] have shown clinical applicability but often lack detailed quantitative metrics for direct benchmarking. In contrast, according to results showed in Tables 2 and 3, the proposed XGBoosting model attains RMSE = 6.097 mmHg, MAE = 5.505 mmHg, and $R^2 = 0.928$ for systolic BP, and RMSE = 7.356 mmHg, MAE = 5.704 mmHg, and $R^2 = 0.758$ for diastolic BP. While some traditional methods report lower systolic MAEs, their lack of RMSE and R^2 indices preclude a holistic comparison. Notably, for diastolic BP, Random Forest achieves a slightly higher determination coefficient ($R^2 = 0.781$) than XGBoosting, whereas XGBoosting provides the lowest RMSE. Overall, these results position the proposed model as a competitive alternative for PPG-based BP estimation, with transparent and comprehensive performance reporting aligned with contemporary clinical validation requirements.

The results show that, for systolic blood pressure estimation, the XGBoosting model achieved the best overall performance, with the lowest RMSE (6.097 mmHg) and MAE (5.505 mmHg), together with the highest coefficient of determination (R^2= 0.928). Random Forest delivered very similar results (RMSE = 6.829 mmHg, MAE = 5.514 mmHg, R^2= 0.915), while Back Propagation lagged behind (RMSE = 8.952 mmHg, MAE = 7.194 mmHg, R^2= 0.862). For diastolic blood pressure, the picture is more nuanced: XGBoosting attains the lowest RMSE (7.356 mmHg), Random Forest achieves the highest R^2 (0.781), and Back Propagation yields the lowest MAE (5.666 mmHg). Notably, all models keep diastolic RMSE below 8 mmHg, and the two ensemble methods are also below this threshold for systolic BP, underscoring the practical viability of ensemble approaches for non-invasive BP estimation from PPG signals. When compared to established approaches such as KNN, Bagged Trees, and CNN models based on Korotkoff sounds, our ensemble-based methods stand out for providing not only competitive accuracy but also a more complete evaluation by reporting RMSE and R^2 metrics that are rarely detailed in prior studies. These findings strengthen the case for integrating ensemble learning into IoT-enabled hospital triage systems, highlighting their ability to deliver precise blood pressure estimation and support timely, evidence-based patient prioritization, ultimately enhancing the efficiency and quality of emergency care.

Table 4. Comparison of blood pressure estimation models

Model	RMSE	MAE	R^2	Reference
CNN (Korotkoff Sounds)	--	Not reported	--	Korotkoff
KNN Systolic	--	3.590	--	KNN
Weighted KNN Systolic	--	3.520	--	KNN
Bagged Trees Systolic	--	4.499	--	KNN

Model	RMSE	MAE	R^2	Reference
Back Propagation Systolic	8.952	7.194	0.862	This paper
XGBoosting Systolic*	6.097	5.505	0.928	This paper
Random Forest Systolic	6.829	5.514	0.915	This paper
Back Propagation Diastolic	7.840	5.666	0.712	This paper
XGBoosting Diastolic*	7.356	5.704	0.758	This paper
Random Forest Diastolic	7.621	5.921	0.781	This paper

5. Conclusion

The main contribution of this paper is to train and evaluate the algorithms XGBoost, random forests, and deep neural networks to estimate blood pressure, considering demographic and comorbidity data, vital-sign measurements, and wearable device indices derived from PPG signals. In this context, a novelty is the applicability of a proposed system to complement triage in isolated regions where there is a lack of experts to support health personnel, using machine learning to predict patients' health status. The results show that, for systolic and diastolic blood pressure estimation, the XGBoost model achieved the lowest RMSE and the highest coefficient of determination compared with the other considered algorithms, indicating an acceptable error and a suitable fit of the learning model. These ensemble models achieved RMSE values below the 8 mmHg threshold, often cited in the AAMI standard, highlighting their clinical relevance. We recommend using XGBoost to estimate systolic and diastolic blood pressure from PPG signal features combined with demographic information. Furthermore, we emphasize that this type of estimation is valid for triage in isolated regions with limited specialized personnel. In future research, we focus on strengthening clinical robustness through external validation, multisite studies, and diverse subject cohorts, and on methods to remove motion artifacts from PPG signals.

Declarations

Author Contributions

Author Contributions: Conceptualization, Joel Carroll Vargas, Andrés Jutinico and Edwin Reyes; methodology, Joel Carroll Vargas; software, Joel Carroll Vargas; validation, Joel Carroll Vargas, Andrés Jutinico and Edwin Reyes; formal analysis, Joel Carroll Vargas; investigation, Joel Carroll Vargas; resources, Andrés Jutinico and Edwin Reyes; data curation, Joel Carroll Vargas; writing—original draft preparation, Joel Carroll Vargas; writing—review and editing, Joel Carroll Vargas, Andrés Jutinico and Edwin Reyes; visualization, Joel Carroll Vargas; supervision, Andrés Jutinico and Edwin Reyes; project administration, Andrés Jutinico; funding acquisition, Andrés Jutinico and Edwin Reyes. All authors have read and agreed to the published version of the manuscript.

Funding

The authors appreciate the financial support provided by UAN (Investment Project BPIN 2021000100014 from the Bicentennial Doctoral Excellence Scholarship Program) and Minciencias during the development of this study.

Acknowledgements

The authors sincerely acknowledge the support of the Universidad Antonio Nariño and its Doctoral Program in Applied Sciences.

Institutional Review Board Statement

Institutional Review Board Statement. The study was conducted in accordance with the Declaration of Helsinki and approved by the Institutional Review Board (Ethics Committee) of the Universidad Antonio Nariño (protocol code 0005-25 and date of approval: [20 May 2025]).

Conflicts of Interest

The authors declare no conflict of interest. All ethical standards regarding plagiarism, informed consent, data integrity, and publication practices have been fully respected throughout the conduct and reporting of this study.

References

[1] M. Bednarek-Chałuda, A. Żadło, N. Antosz, and P. Clutter, "Polish Perspective: The Influence of National Emergency Severity Index Training on Triage Practitioners' Knowledge," J Emerg Nurs, vol. 50, no. 3, pp. 413–424, 2024.

[2] R. El-Bouri, D. W. Eyre, P. Watkinson, T. Zhu, and D. A. Clifton, "Hospital admission location prediction via deep interpretable networks for the year-round improvement of emergency patient care," IEEE J Biomed Health Inform, vol. 25, no. 1, pp. 289–300, 2020.
[3] D. Olivia, C. Amrutha, A. Nayak, M. Balachandra, and A. Saxena, "Clinical severity level prediction based optimal medical resource allocation at mass casualty incident," IEEE Access, vol. 10, pp. 88970–88984, 2022.
[4] N. Gilboy, P. Tanabe, D. Travers, A. M. Rosenau, and others, "Emergency Severity Index (ESI): a triage tool for emergency department care, version 4," Implementation handbook, vol. 2012, pp. 12–14, 2012.
[5] Colombia. Ministerio de Salud y Protección Social, "Resolución número 5596 de 2015," 2015, Bogotá. [Online]. Available: https://www.minsalud.gov.co/sites/rid/Lists/BibliotecaDigital/RIDE/DE/DIJ/resolucion-5596-de-2015.pdf
[6] R. C. Wuerz, L. W. Milne, D. R. Eitel, D. Travers, and N. Gilboy, "Reliability and validity of a new five-level triage instrument," Academic emergency medicine, vol. 7, no. 3, pp. 236–242, 2000.
[7] L. Burgess, K. Kynoch, and S. Hines, "Implementing best practice into the emergency department triage process," JBI Evid Implement, vol. 17, no. 1, pp. 27–35, 2019.
[8] P. Williams et al., "Efficacy of a triage system to reduce length of hospital stay," The British Journal of Psychiatry, vol. 204, no. 6, pp. 480–485, 2014.
[9] A. Khorram-Manesh, K. Lennquist Montán, A. Hedelin, M. Kihlgren, and P. Örtenwall, "Prehospital triage, discrepancy in priority-setting between emergency medical dispatch centre and ambulance crews," European Journal of Trauma and Emergency Surgery, vol. 37, no. 1, pp. 73–78, 2011.
[10] T. Ullah, "Analysis Of Factors That Affect the Implementation Of Triage On Satisfaction Of Patients Family," Journal of Applied Nursing and Health, vol. 4, no. 1, pp. 140–145, 2022.
[11] I. Kuzmanov, A. M. Bogdanova, M. Kostoska, and N. Ackovska, "Fast cuffless blood pressure classification with ECG and PPG signals using CNN-LSTM models in emergency medicine," in 2022 45th Jubilee International Convention on Information, Communication and Electronic Technology (MIPRO), 2022, pp. 362–367.
[12] S. Sarkar and S. K. Pahuja, "Current developments in cuff-free non-invasive continuous blood pressure estimation using photoplethysmography," Biomedical Materials & Devices, vol. 2, no. 2, pp. 743–758, 2024.
[13] M. R. Shaikh and M. Forouzanfar, "Dual-stream CNN-LSTM architecture for cuffless blood pressure estimation from PPG and ECG signals: A PulseDB study," IEEE Sens J, 2024.
[14] F. Pan, P. He, F. Chen, J. Zhang, H. Wang, and D. Zheng, "A novel deep learning based automatic auscultatory method to measure blood pressure," Int J Med Inform, vol. 128, pp. 71–78, 2019.
[15] A. S. Alghamdi, K. Polat, A. Alghoson, A. A. Alshdadi, and A. A. Abd El-Latif, "A novel blood pressure estimation method based on the classification of oscillometric waveforms using machine-learning methods," Applied Acoustics, vol. 164, p. 107279, 2020.
[16] Organización Panamericana de la Salud, "Manual para la implementación de un sistema de triaje para los cuartos de urgencias," 2011.
[17] L.-H. Wang, K.-K. Sun, C.-X. Xie, M.-H. Fan, P. A. R. Abu, and P.-C. Huang, "Cuffless blood pressure estimation using dual physiological signal and its morphological features," IEEE Sens J, vol. 23, no. 11, pp. 11956–11967, 2023.
[18] Q. Wan et al., "Toward Real-Time Blood Pressure Monitoring via High-Fidelity Iontronic Tonometric Sensors with High Sensitivity and Large Dynamic Ranges," Adv Healthc Mater, vol. 12, no. 17, p. 2202461, 2023.
[19] B. Tarifi, A. Fainman, A. Pantanowitz, and D. M. Rubin, "A machine learning approach to the non-invasive estimation of continuous blood pressure using photoplethysmography," Applied Sciences, vol. 13, no. 6, p. 3955, 2023.
[20] A. Garrett et al., "Simultaneous photoplethysmography and blood flow measurements towards the estimation of blood pressure using speckle contrast optical spectroscopy," Biomed Opt Express, vol. 14, no. 4, pp. 1594–1607, 2023.
[21] P.-K. Man et al., "Blood pressure measurement: From cuff-based to contactless monitoring," in Healthcare, 2022, p. 2113.
[22] S. K. Nadar and Y. V Gregory, Hypertension (Oxford Cardiology Library), 3rd ed. OUP Oxford, 2023.
[23] Y. Liang, Z. Chen, G. Liu, and M. Elgendi, "A new, short-recorded photoplethysmogram dataset for blood pressure monitoring in China," Sci Data, vol. 5, no. 1, pp. 1–7, 2018.
[24] P. Mehrgardt, M. Khushi, S. Poon, and A. Withana, "Pulse Transit Time PPG Dataset," 2022. [Online]. Available: https://physionet.org/content/pulse-transit-time-ppg/1.1.0/
[25] T. Chen and C. Guestrin, "Xgboost: A scalable tree boosting system," in Proceedings of the 22nd acm sigkdd international conference on knowledge discovery and data mining, 2016, pp. 785–794.

参考文:

[1] M. Bednarek-Chałuda, A. Żadło, N. Antosz, 和 P. Clutter，“波兰视角：国家急诊严重指数培训对分诊人员知识的影响，”《急诊护理杂志》，第50卷，第3期，页413–424，2024年。

[2] R. El-Bouri, D. W. Eyre, P. Watkinson, T. Zhu, 和 D. A. Clifton，“通过可解释深度网络预测医院入院位置以全年改善急诊患者护理，”《IEEE生物医学与健康信息学杂志》，第25卷，第1期，页289–300，2020年。

[3] D. Olivia, C. Amrutha, A. Nayak, M. Balachandra, 和 A. Saxena，“基于临床严重等级预测的质量伤亡事件最优医疗资源分配，”《IEEE Access》，第10卷，页88970–88984，2022年。

[4] N. Gilboy, P. Tanabe, D. Travers, A. M. Rosenau, 等，“急诊严重指数（ESI）：急诊科分诊工具，第4版，”实施手册，第2012卷，页12–14，2012年。

[5] 哥伦比亚卫生与社会保障部，“2015年第5596号决议，”2015年，波哥大。[在线]。可访问：https://www.minsalud.gov.co/sites/rid/Lists/BibliotecaDigital/RIDE/DE/DIJ/resolucion-5596-de-2015.pdf

[6] R. C. Wuerz, L. W. Milne, D. R. Eitel, D. Travers, 和 N. Gilboy，“一种新的五级分诊工具的可靠性和有效性，”《学术急诊医学》，第7卷，第3期，页236–242，2000年。

[7] L. Burgess, K. Kynoch, 和 S. Hines，“将最佳实践应用于急诊科分诊流程，”《JBI证据实施》，第17卷，第1期，页27–35，2019年。

[8] P. Williams 等，“一种分诊系统降低住院时间的有效性，”《英国精神病学杂志》，第204卷，第6期，页480–485，2014年。

[9] A. Khorram-Manesh, K. Lennquist Montán, A. Hedelin, M. Kihlgren, 和 P. Örtenwall，“院前分诊：急救调度中心与救护车队伍优先级设置的差异，”《欧洲创伤与急诊外科杂志》，第37卷，第1期，页73–78，2011年。

[10] T. Ullah，“影响分诊实施对患者家属满意度的因素分析，”《应用护理与健康杂志》，第4卷，第1期，页140–145，2022年。

[11] I. Kuzmanov, A. M. Bogdanova, M. Kostoska, 和 N. Ackovska，“在急诊医学中使用CNN-LSTM模型通过ECG和PPG信号实现快速无袖带血压分类，”收录于《2022年第45届信息、通信与电子技术国际大会（MIPRO）》，2022年，页362–367。

[12] S. Sarkar 和 S. K. Pahuja，“光电容积描记法非接触连续血压估算的最新进展，”《生物医学材料与器械》，第2卷，第2期，页743–758，2024年。

[13] M. R. Shaikh 和 M. Forouzanfar，“基于PPG和ECG信号的无袖带血压估算双流CNN-LSTM架构：PulseDB研究，”《IEEE传感器杂志》，2024年。

[14] F. Pan, P. He, F. Chen, J. Zhang, H. Wang, 和 D. Zheng，“一种基于深度学习的新型自动听诊血压测量方法，”《国际医学信息学杂志》，第128卷，页71–78，2019年。

[15] A. S. Alghamdi, K. Polat, A. Alghoson, A. A. Alshdadi, 和 A. A. Abd El-Latif，“一种基于机器学习方法分类振荡波形的新型血压估算方法，”《应用声学》，第164卷，文章编号107279，2020年。

[16] 泛美卫生组织，“急诊室分诊系统实施手册，”2011年。

[17] L.-H. Wang, K.-K. Sun, C.-X. Xie, M.-H. Fan, P. A. R. Abu, 和 P.-C. Huang，“利用双生理信号及其形态特征进行无袖带血压估算，”《IEEE传感器杂志》，第23卷，第11期，页11956–11967，2023年。

[18] Q. Wan 等，“通过高保真离子计声学传感器实现高灵敏度和大动态范围的实时血压监测，”《先进医疗材料》，第12卷，第17期，文章编号2202461，2023年。

[19] B. Tarifi, A. Fainman, A. Pantanowitz, 和 D. M. Rubin，“利用光电容积描记法进行连续血压非侵入估算的机器学习方法，”《应用科学》，第13卷，第6期，文章编号3955，2023年。

[20] A. Garrett 等，“同时进行光电容积描记和血流测量以通过散斑对比光学光谱估算血压，”《生物医学光学快报》，第14卷，第4期，页1594–1607，2023年。

[21] P.-K. Man 等，“血压测量：从袖带到非接触监测，”收录于《医疗保健》，2022年，文章编号2113。

[22] S. K. Nadar 和 Y. V Gregory，《高血压（牛津心脏病学图书馆）》，第3版，牛津大学出版社，2023年。
[23] Y. Liang, Z. Chen, G. Liu, 和 M. Elgendi，“中国血压监测的新型短记录光电容积描记数据集，”《科学数据》，第5卷，第1期，页1–7，2018年。
[24] P. Mehrgardt, M. Khushi, S. Poon, 和 A. Withana，“脉搏传导时间PPG数据集，”2022年。[在线]。可访问：https://physionet.org/content/pulse-transit-time-ppg/1.1.0/
[25] T. Chen 和 C. Guestrin，“XGBoost：可扩展的树增强系统，”收录于《第22届ACM SIGKDD国际知识发现与数据挖掘会议论文集》，2016年，页785–794。

Manuscript Information
Word count: 8,650 words (excluding references).

Peer-Review Record
Fast-track status: Not fast-tracked.
First-round reviews received: 3 reports.
Revision cycles completed: 3 rounds.
Final version submitted: February 24, 2026